Shunt Quenching and Concept of Independent Global Shunt in Multijunction Solar Cells

Federico Ventosinos, Jan Klusáček, Tomáš Finsterle, Karel Künzel, Franz-Josef Haug, and Jakub Holovský

***Abstract*—We show that two-terminal multijunction cells interconnected by tunnel junctions are fairly immune to individual local shunts, thanks to the shunt quenching. Interestingly, they may still suffer from global shunts. We revise the paradigm of a multijunction cell as a simple serial connection of component cells. This paradigm remains valid only for multijunction cells with laterally conductive interlayers. Instead, a new equivalent circuit is proposed and verified by measurement and simulations. As a main approach, selective illumination is applied and the voltage is measured at the end terminals. The global shunt is seen as a shift from logarithmic to linear intensity response. The presence of tunnel junction is important for an optimum configuration of tandem structures such as metal-halide perovskite with crystalline silicon solar cell.**

***Index Terms*—Equivalent circuit, multijunction solar cells, shunting, solar cells, tandem solar cells, tunnel junction.**

I. Introduction

AS THE efficiencies of the record laboratory solar cells are approaching their theoretical maximum given by the Shockley–Queisser limit, the next step will naturally be the combination of different absorbers into a multijunction cell. Finding technologically compatible materials allowing well-balanced photogenerated current is challenging. Therefore, in tandem cells, a four-terminal architecture of two separate cells, both of them having their own pair of collecting electrodes, is sometimes used [1], [2]. However, the existence of unnecessary internal laterally conductive layers increases the optical losses and limits the efficiency. The ultimate concept should therefore contain only front and back laterally conductive electrodes, and only tunnel junctions in between the individual subcells [3], [4]. This is the concept used in record III–V quadruple cells as well as tandem amorphous-microcrystalline silicon solar cells. The latter technology has been well-developed commercially, mainly due to the easy combination of the two different materials in one technological tool [5]. The tunnel junction interconnection is realized as very thin p+/n+ tunnel diode with high saturation current imposing only negligible voltage loss.

In thin-film cells, the sheet conductivity of doped layers is usually not high enough to collect the current, therefore a transparent conductive oxide (TCO) is used as the electrode. Often, the TCO is deliberately prepared to have a rough surface in order to scatter light. This roughness on the other hand may negatively affect the subsequent growth of absorber material, leading to point defects. To describe the situation electronically, a mesh of diodes instead of a single diode has been suggested [6]. This has proven to be very useful for describing an effect of so-called shunt-quenching that counterintuitively uses a resistive layer to improve *I–V* characteristics [7]. The hypothesis of such shunt quenching is that a shunt can only be effective if the current from a large area can be drained [see Fig. 1(a)]. If only the current from the close vicinity can be drained, the shunt is relatively benign. In this concept, the thin resistive layer does not prevent shunting, but prevents draining current from a larger surrounding area [8] [see Fig. 1(b)]. Similarly, if in a tandem each individual subcell has some *local* shunts that use the front or back electrode on the outer sides and the p+/n+ tunneling interface between the cells, these shunts are benign because the lateral conductivity of p+/n+ layers is small [see Fig. 1(c)]. If such shunts from each subcell meet each other, they can create a *global* shunt connecting the front and back electrode with high conductivity. Therefore, this shunt is detrimental [see Fig. 1(d)].

In this paper, we give evidence for the existence of *global* shunts and show that such a detrimental *global* shunt can in principle be composed of only benign *local* shunts.

II. Experimental Techniques

The accurate determination of the equivalent circuit is important for understanding the relationships between the *I–V* curve of a multijunction cell, its component contributions, and the design of efficient solar cells. A variety of methods exist for determining the component *I–V* curves in tandem cells [9]–[16]. These

Manuscript received February 16, 2018; accepted March 28, 2018. Date of publication June 4, 2018; date of current version June 19, 2018. This work was supported in part by the Czech Ministry of Education, Youth and Sports projects LTC17029 INTER-COST Action MP1406 and no. CZ.02.1.01/0.0/0.0/15_003/0000464 Centre of Advanced Photovoltaics, in part by Czech Academy of Sciences project NANOCELL KONNECT-007, and in part by student project no. SGS16/077/OHK3/1T/13. *(Corresponding author: Jakub Holovský.)*

F. Ventosinos is with the École Polytechnique, LPICM, UMR 7647, CNRS, Palaiseau F-91128, France, and also with the Faculty of Electrical Engineering, Czech Technical University in Prague, Prague 166 27, Czech Republic (e-mail: fedevento@gmail.com).

J. Klusáček is with the Institute of Physics, Czech Academy of Sciences, v. v. i., Prague 162 00, Czech Republic (e-mail: jan.klusacek@mail.muni.cz).

T. Finsterle and K. Künzel are with the Faculty of Electrical Engineering, Czech Technical University in Prague, Prague 166 27, Czech Republic (e-mail: tomfin@centrum.cz; kuenzel@fel.cvut.cz).

F.-J. Haug is with the Photovoltaics and Thin Film Electronics Laboratory, Institute of Microengineering, École Polytechnique Fédérale de Lausanne, Neuchâtel CH-2002, Switzerland (e-mail: franz-josef.haug@epfl.ch).

J. Holovský is with the Faculty of Electrical Engineering, Czech Technical University in Prague, Prague 166 27, Czech Republic, and also with the Institute of Physics, Czech Academy of Sciences, v. v. i., Prague 162 00, Czech Republic (e-mail: holovsky@fzu.cz).

Color versions of one or more of the figures in this paper are available online at http://ieeexplore.ieee.org.

Digital Object Identifier 10.1109/JPHOTOV.2018.2828850

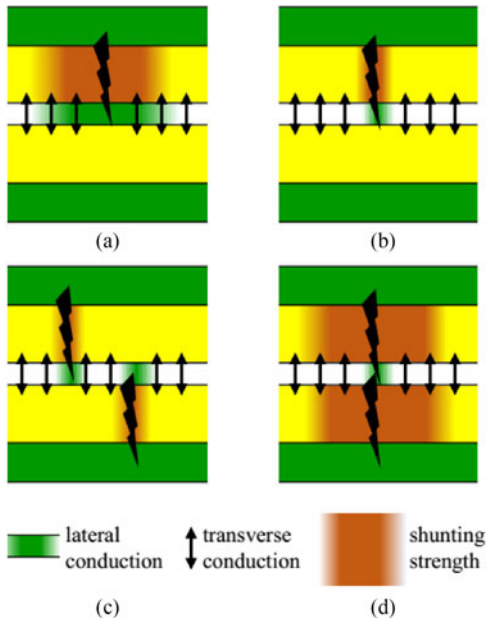

Fig. 1. Effect of the existence of laterally conductive layer on the strength of shunts. (a) Effective local shunt. (b) Local shunt quenched by the lack of a laterally conductive interlayer. (c) Two benign local shunts. (d) Two local shunts creating one effective global shunt.

methods, however, assume the tandem device to be two serially connected cells. In such a case, the voltage of the tandem solar cell is the sum of the two voltages induced on the component subcells. Strictly speaking, this is valid only for the case with a highly laterally conductive layer in between the component subcells. Usually, open-circuit voltage (V_{OC}) is a logarithmic function of the photogenerated carrier density. Measurement of illumination-V_{OC} curve is a method giving so-called pseudo *I–V* curve that, for typical device, resembles the *I–V* curve without the effect of serial resistance [17].

As we are not focused on serial resistance effects here, it is plausible to also use illumination-V_{OC} for the assessment of the device operation at standard test conditions, including evaluation of the fill factor, as seen in Fig. 3.

The cells used in this study were single amorphous silicon (a-Si), single microcrystalline (μc-Si) and tandem a-Si/μc-Si solar cells. Two standard cells featuring usual p+/n+ tunnel junctions were prepared. The tunnel junction cells are labeled #1 and #2, and are from the same deposition batch, but exhibit completely different behavior due to different levels of shunting. In Fig. 3, we also present a sample with conductive ZnO interlayer, whose purpose is to show the case in which the paradigm of serial connection is valid. This sample is not used for the following simulations, as shunt quenching is not present within it. All cells were deposited on boron doped ZnO substrates by plasma-enhanced chemical vapor deposition from SiH_4 diluted by H_2 gas. More details can be found in [18].

In order to induce the measured voltages across the cells, we illuminated them with a narrow angle blue light emitting diode arrays (LED) ($\lambda = 470$ nm, $\phi = 5$ mm, $\Phi = 160$ mW/sr, 15 pieces) for the a-Si cell and narrow angle infrared (IR) LED ($\lambda = 850$ nm, $\phi = 5$ mm, $\Phi = 700$ mW/sr, 24 pieces) for μc-Si

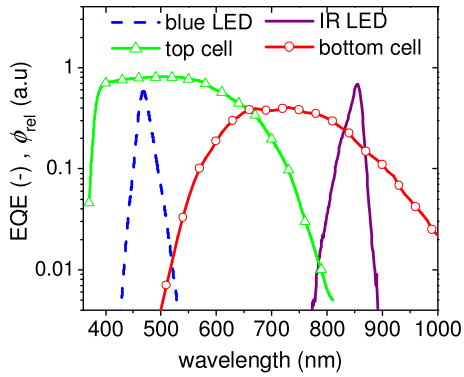

Fig. 2. EQE curves of top and bottom component subcells of an amorphous-microcrystalline silicon tandem solar cell and photon emission spectra of the LED illumination system.

cell. The two LEDs were driven through a computer-controlled current source to homogeneously illuminate an area of 0.4 cm^2 defined by a mask. In Fig. 2 we show the spectral distribution of the LEDs, compared to the typical external quantum efficiency (EQE) of the a-Si/μc-Si tandem device. This set-up allows for selective illumination, i.e., the ability to generate voltage preferentially in one selected subcell. However, the selective generation of voltage will never be perfect, because voltage is logarithmically dependent on the generation. This means that even a small unwanted photogeneration raises the V_{OC} considerably. The problem of selectivity was thoroughly treated in our previous paper [14], mainly by sweeping the blue and/or infrared LED illumination intensity from 0 to the equivalent of 1 sun, followed by mathematical simulations. The same approach is applied to understand the effect of shunt distribution here.

III. Results

A. Voltage Measurement

The sweeps of LED intensity going from 0 to 1 sun were performed, while the voltage on the terminals was recorded. The sweeps of the blue LEDs, the IR LEDs, and both combined give the experimental voltage sequences $v_{\text{blue exp}}$, $v_{\text{IR exp}}$, and $v_{\text{comb exp}}$, respectively. The voltage behavior of tested cells could be divided into three groups, shown in Fig. 3. On the left side, the measurement of the sample with the conductive interlayer is shown. Both subcells show the typical logarithmic behavior expected for the increasing illumination intensity. However, they still exhibit the problem with the weak selectivity such that the contribution from parasitic absorption appears (absorption of blue light in the μc-Si subcell and absorption of IR LED in the a-Si subcell). This makes the sum of the individual curves higher than the voltage measured under illumination from both LEDs combined.

The sample with tunnel junction labeled #1 shows a similar effect of weak selectivity, as the sum of individual illuminations (orange flipped triangles) is higher than the curve showing the combined illumination (black squares). However, at intensities below 0.4 suns, the two curves cross, which indicates the important effect related to the global shunt.

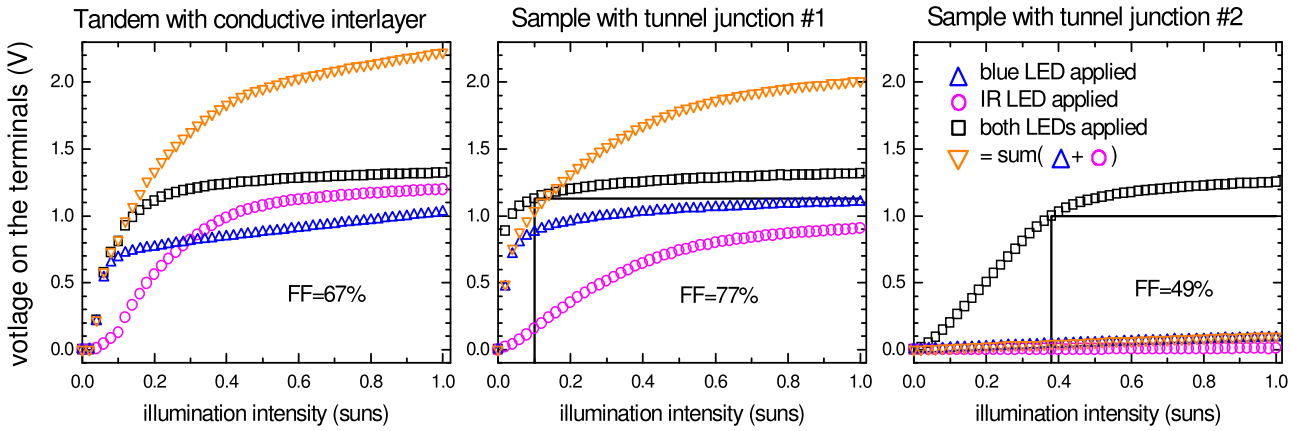

Fig. 3. Different behaviors of the measured V_{OC} when selectively illuminating the cells. In the case with a conductive interlayer, the voltages of subcells add together, but the numerically calculated sum is larger due to additional parasitic absorption. Sample #1 represents a similar case, but in the low intensity range the numerically calculated sum is smaller than the measurement under both LEDs, as if the mc-Si:H subcell was shunted. However, the measurement under both LEDs does not show the effect of such a shunt. The extreme case is sample #2, which represents a considerably shunted tandem cell, but not as much as the measurements under selective illumination would suggest.

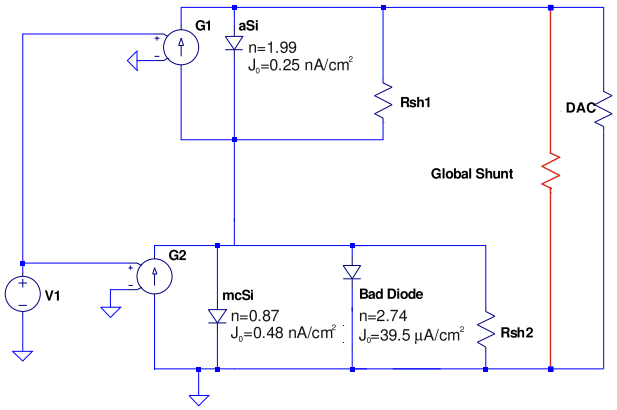

Fig. 4. Tandem solar cell equivalent circuit model for simulating illumination sweeps and external voltage measurement. The global shunt is drawn in red. The numerical values are the values obtained from tests made on single cells in the first step.

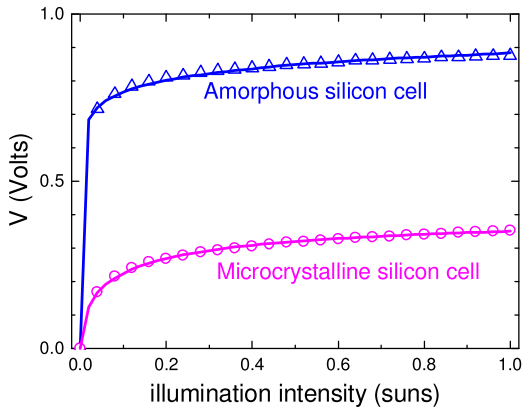

Fig. 5. Single cell voltage measurements (triangles for a-Si:H and circles for mc-Si:H), with lines representing the simulations of the single cells using the best parameters found.

The effect of the global shunt in its full strength is observed in the sample with tunnel junction labeled #2, where the curves taken under individual LED illumination are very low. The global shunt is drawn in red in Fig. 4. The hypothesis is that together with data acquisition unit, it acts more like an ammeter, shifting the operation of the solar cells from open-circuit (high load resistance) to short-circuit (low load resistance) condition. In such a case, the measured signal corresponds to current and becomes limited by the cell with the lower photogenerated current. That explains why the signals with only one LED (circles and triangles) are very low, while the signal with both LEDs (squares) has the usual shape of a device (with considerable shunt).

B. Equivalent Circuit

In order to prove the hypothesis, we simulated the voltage as a function of the illumination intensity using the equivalent circuit model shown in Fig. 4. As can be seen, the equivalent circuit of the tandem device consists of two single cells (the a-Si cell on top and the μc-Si on the bottom). Serial resistance is not included, as its effect is negligible in the V_{OC} measurement. G_1 and G_2 are voltage-driven sources of current that simulate the photogenerated current due to LED illumination. Both single cell models contain a local shunt resistance R_{sh}. In the bottom microcrystalline cell, an extra so-called *bad diode* is included to account for cracks [18].

The *global shunt* is shown in red. Finally, the *DAC* represents the data acquisition unit NI USB-6008 with input impedance of 144 kΩ for the voltage measurement.

The diodes *a-Si* and *mc-Si* are each defined by a saturation current J_0, and ideality factor n. The response to the blue and IR LEDs is defined by the dimensionless parameters g_{11} and g_{12}, respectively, for the top cell and g_{21} and g_{22} for the bottom cell. The photogenerated currents G_i for $i = 1,2$ are then calculated as $G_i = 10\,\text{mA/cm}^2 \cdot (g_{i1}\Phi_{\text{blue}} + g_{i2}\Phi_{\text{IR}})$, where Φ_{blue}, Φ_{IR} are

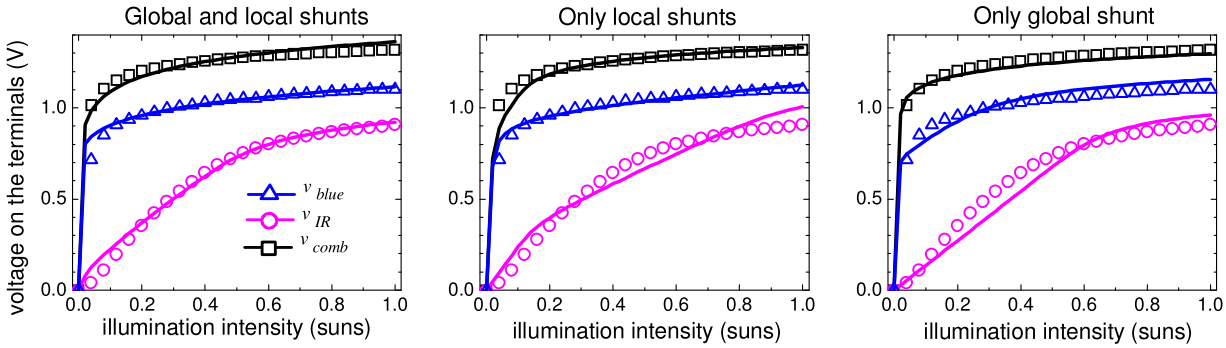

Fig. 6. Results of the optimization of different models for sample #1. On the left side we used the model that includes both local and global shunts, in the middle, no global shunts were used, while on the right side the local shunts were removed.

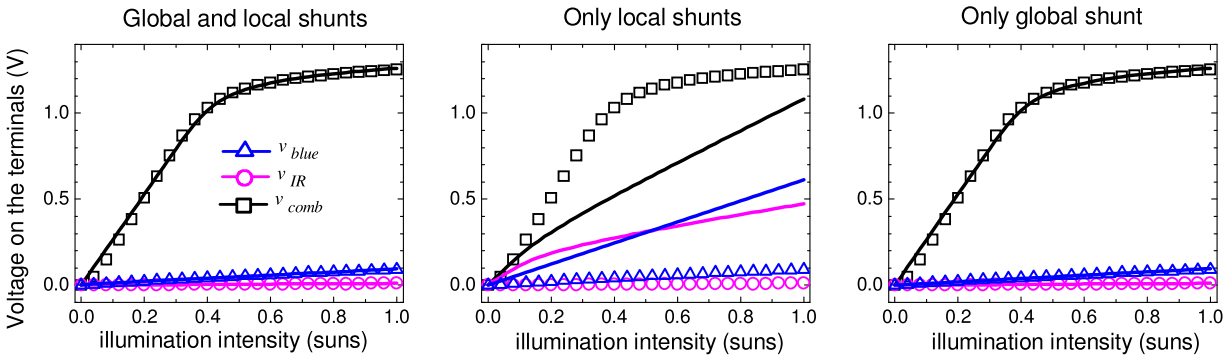

Fig. 7. Result of the optimization of different models from sample #2. On the left side we used the model that includes both local and global shunts, in the middle, no global shunts were used and the fitting procedure was unsuccessful, while on the right side the local shunts were removed.

dimensionless variables between 0 and 1 (1 sun), expressing the blue and IR diode illumination intensity. The photogeneration is normalized to give 10 mA/cm^2 when the LEDs are operated at full intensity ($g_{ii} = 1$), assuming perfect selectivity ($g_{ij} = 0$ for $i \neq j$).

C. Parameter Optimization

We programmed an optimization routine that calls MATLAB Simulink to run the circuit simulation, while the parameter optimization is done in MATLAB by comparing the simulation results with the experimental values. MATLAB Simulink runs sweeps of Φ_{blue}, and Φ_{IR}, or both from 0 to 1 and records the voltage sequences $v_{\text{blue sim}}$, $v_{\text{IR sim}}$, and $v_{\text{comb sim}}$ at the *DAC*. MATLAB builds and minimizes a test function f, defined as $f^2 = (v_{\text{blue sim}} - v_{\text{blue exp}})^2 + (v_{\text{IR sim}} - v_{\text{IR exp}})^2 + (v_{\text{comb sim}} - v_{\text{comb exp}})^2$, by varying the fit parameters. For this purpose, we employed MATLAB's function `fminsearch`. Considering the large number of parameters to fit, we divided the fitting procedure into two steps.

First, we used models of single cell devices and sweeps of only one LED to get a good starting point on the a-Si and μc-Si cells parameters. The result of that calibration is shown in Fig. 5. As can be seen, the single cell simulations have great agreement with the measurements. The values found for all the diodes are in fair agreement with literature values and are indicated in Fig. 4.

Second, for the full simulations of the tandem cell, we fixed the values of ideality factors and set g_{11} and g_{22} either to 1 or 0 depending on the measurement conditions, while optimizing local and/or global shunt resistances, selectivity parameters g_{12} and g_{21}, and the diode saturation currents J_{S1}, J_{S2a}, and J_{S2b}. In order to understand the influence of each resistance, we used three different equivalent circuit models in the optimization, one that includes both local and global shunts (see the left side of Figs. 6 and 7), one without the influence of the global shunt (see the central graph of Figs. 6 and 7) and one with a global shunt but without the local shunts.

Looking at the quality of the fit, we can conclude that the proposed equivalent circuit reproduces the experimental data sufficiently well when the global shunt is present. We can especially clearly see that the global shunt is a necessary component while the local shunts can be removed completely. Fitted values of local shunts and global shunts are shown in Table I.

In the case of sample #1 featuring only a weak global shunt, the cells are close to open-circuit conditions and the voltage is not far from the sum of component voltages, as in the case of serially connected photodiodes. The usual logarithmic shape of illumination-dependent V_{OC} can be observed. The effects of considering only local shunts or only global shunts are similar.

On the other hand, in the case of sample #2, with a strong global shunt the cells are close to short-circuit conditions, where the dependence on illumination is linear and the tandem cell is in a regime when the photocurrent is limited by the subcell generating less current. The observed behavior can be reproduced by an alternative model of a voltage divider: Current generated

TABLE I
VALUES OBTAINED BY THE OPTIMIZATION ROUTINE

		Top Cell			Bottom Cell			Tandem
		J_s (mA/cm^2)	g_{12} (%) (i.r. abs. in top cell)	Local shunt resistance ($k\Omega cm^2$)	J_{s1}, J_{s2} (mA/cm^2)	g_{21} (%) (blue abs. in bottom cell)	Local shunt resistance ($k\Omega cm^2$)	Global Shunt Resistance ($k\Omega cm^2$)
# 1 (Fig. 6)	global and local shunts	2.7×10^{-8}	0.04	518	1.2×10^{-13}, 0.05	2.4	10^{28}	552
	only local shunts	1.6×10^{-8}	2.1	3.6	7.0×10^{-6}, 8.1×10^{-4}	6.4	0.16	∞
	only global shunt	1.3×10^{-9}	0.45	∞	0.012 , 0.011	0.44	∞	30
# 2 (Fig. 7)	global and local shunts	9.2×10^{-8}	0.39	10^{17}	4.9×10^{-7}, 1.3×10^{-4}	3.4	10^{6}	0.26
	only global shunt	8.9×10^{-8}	0.39	∞	1.7×10^{-2}, 1.3×10^{-4}	3.7	∞	0.26

by the illuminated subcell creates voltage on the shunt resistor of nonilluminated subcells, and on the global shunt resistor. The ratio of these voltages is equal to the ratio of the resistors. This can be cross-checked by analyzing results of sample #2 in Table I. Because local shunts are either inactive or negligible, the current flowing through the global shunt must be equal to the generated current. The generated current is limited by the values g_{12}, g_{22} (assuming that 100% corresponds to 10 mA). Then, a value of 0.39% IR light absorbed in the top cell gives 0.039 mA. This current is converted to 0.01 V by the 0.26 kΩ of the global shunt. This 0.01 V is the value measured on the sample #2 with full IR light, as seen in Fig. 7. Correspondingly, 3.7% of blue light absorbed in the top cell gives 0.37 mA, and is converted to 0.1 V by the 0.26 kΩ of the global shunt. This 0.1 V is the value measured on the sample #2 with full blue light. This means that the flatness of the curves obtained with selective illumination for sample #2 as well as sloped beginning of the curve under the IR LED for sample #1 is not due to local shunt resistance, as they may appear to be, but due to global shunt resistance combined with the selectivity factor. The value of the local shunt therefore cannot be determined directly just from the slope of individual curves.

This proves the hypothesis that in the thin-film multijunction devices without a conductive interlayer, the global shunt may exist even without any observable local component shunts. It means that if the component subcells have, for example, point defects causing shunts, they are quenched at least on the subcell level. Whether they are quenched also on the global level depends on their spatial distribution. Shunts will only be observed in the case when two (locally quenched) shunts are located at the same point and can combine to create a global shunt.

This implies that isolated local shunts are naturally quenched and therefore remain hidden. Such hidden quenched local shunts have no effect on the operation of solar cell under standard test conditions. Only global shunts have a detrimental effect on the cell operation.

IV. DISCUSSION

The recent emergence of metal-halide perovskite solar cells is especially important as a perspective top cell for a tandem solar cell with a crystalline silicon bottom subcell. From the perspective of shunt quenching studied here, the preferred structure of the bottom cell is the one without a laterally conductive layer in the front. This can be realized with silicon heterojunction technology. Namely, for the standard deposition sequence of a perovskite cell starting with the electron transporting material, the recommended configuration would be an n-type wafer with p-type contact in front. Conversely, for the perovskite solar cell using an inverted sequence starting with the hole transporting material, the preferred configuration would be n-type contact in front and a p-type wafer. The common rule is that majority carriers should not be collected at the side of the tunnel junction, because like that they could more easily flow to the points of local shunts.

V. CONCLUSION

Comparing the voltage of the multijunction solar cell measured under white light and under selective illumination can help determine the equivalent circuit of the device. If the selectivity of the illumination is strong enough, then the existence of the parallel global shunt is unambiguously revealed when the sum of the measured voltages for selective illumination is less than the voltage measured with white light.

This experiment reveals that in technologies using a tunnel junction local shunt is naturally quenched due to the lack of an intermediate conductive layer. This has positive impact on operation of the device at standard test conditions. Unfortunately, when local shunts in both subcells are close together, they create an active global shunt, which drains current through the laterally conductive layers that are in principle always present on the front and back of the tandem device.

Conclusions can be made about the preferred configuration of metal-halide perovskite—silicon heterojunction tandem solar cells.

ACKNOWLEDGMENT

J. Holovský would like to thank E. Feuser for help with sample exchange.

REFERENCES

[1] J. Werner *et al.*, "Efficient near-infrared-transparent perovskite solar cells enabling direct comparison of 4-terminal and monolithic perovskite/silicon tandem cells," *ACS Energy Lett.*, vol. 1, no. 2, pp. 474–480, Aug. 2016.

[2] M. A. Green, M. J. Keevers, I. Thomas, J. B. Lasich, K. Emery, and R. R. King, "40% efficient sunlight to electricity conversion: Sunlight to electricity conversion efficiency above 40%," *Prog. Photovolt., Res. Appl.*, vol. 23, no. 6, pp. 685–691, Jun. 2015.

[3] M. Boccard *et al.*, "High-stable-efficiency tandem thin-film silicon solar cell with low-refractive-index silicon-oxide interlayer," *IEEE J. Photovolt.*, vol. 4, no. 6, pp. 1368–1373, Nov. 2014.
[4] H. Sai *et al.*, "Triple-junction thin-film silicon solar cell fabricated on periodically textured substrate with a stabilized efficiency of 13.6%," *Appl. Phys. Lett.*, vol. 106, no. 21, May 2015, Art. no. 213902.
[5] J. S. Cashmore *et al.*, "Record 12.34% stabilized conversion efficiency in a large area thin-film silicon tandem (MICROMORPH^{TM}) module: 12.34% stabilized efficiency in a large area module," *Prog. Photovolt., Res. Appl.*, vol. 23, no. 11, pp. 1441–1447, Nov. 2015.
[6] M. Despeisse *et al.*, "Low-conductivity doped layers for improved performance of thin film silicon solar cells on highly textured substrates," in *Proc. 25th Eur. Photovolt. Sol. Energy Conf. Exhib.*, Valencia, Spain, 2010, pp. 2793–2797.
[7] G. Bugnon *et al.*, "A new view of microcrystalline silicon: the role of plasma processing in achieving a dense and stable absorber material for photovoltaic applications," *Adv. Functional Mater.*, vol. 22, no. 17, pp. 3665–3671, Sep. 2012.
[8] M. Despeisse *et al.*, "Resistive interlayer for improved performance of thin film silicon solar cells on highly textured substrate," *Appl. Phys. Lett.*, vol. 96, no. 7, Feb. 2010, Art. no. 073507.
[9] J. Burdick and T. Glatfelter, "Spectral response and I–V measurements of tandem amorphous-silicon alloy solar cells," *Sol. Cells*, vol. 18, pp. 301–314, 1986.
[10] S. Kurtz, K. Emery, and J. M. Olson, "Methods for analysis of two-junction two-terminal photovoltaic devices," in *Proc. 1st World Conf. Photovolt. Energy Convers.*, 1994, pp. 1733–1717.
[11] R. Adelhelm and K. Bücher, "Performance and parameter analysis of tandem solar cells using measurements at multiple spectral conditions," *Sol. Energy Mater. Sol. Cells*, vol. 50, pp. 185–195, Jan. 1998.
[12] Y. Tsuno, Y. Hishikawa, and K. Kurokawa, "Separation of the I-V curve of each component cell of multijunction solar cells," in *Proc. 31st IEEE Photovolt. Spec. Conf.*, 2005, pp. 1476–1479.
[13] C. Das, X. Xiang, and X. Deng, "Method for measuring component cell current-voltage characteristics in a multi-junction, two-terminal stacked solar cell," inHigh Efficiency and High Rate Deposited Amorphous Silicon- Based Solar Cells, NREL Report, NREL/SR-520-39091, 2006, pp. 73–80.
[14] J. Holovsky *et al.*, "Measurement of the open-circuit voltage of individual subcells in a dual-junction solar cell," *IEEE J. Photovolt.*, vol. 2, no. 2, pp. 164–168, Apr. 2012.
[15] J. Holovský, M. Bonnet-Eymard, M. Boccard, M. Despeisse, and C. Ballif, "Variable light biasing method to measure component I–V characteristics of multi-junction solar cells," *Sol. Energy Mater. Sol. Cells*, vol. 103, pp. 128–133, Aug. 2012.
[16] F. Ventosinos, B. Fakes, and E. V. Johnson, "Challenges in advanced characterization techniques for high V_{oc} thin-film tandem solar cells: Advanced characterization techniques for high V_{oc} thin-film tandem solar cells," *Phys. Status Solidi (a)*, vol. 213, no. 7, pp. 1983–1988, Jul. 2016.
[17] M. Wolf and H. Rauschenbach, "Series resistance effects on solar cell measurements," *Adv. Energy Convers.*, vol. 3, pp. 455–479, 1963.
[18] E. Moulin *et al.*, "2-D periodic and random-on-periodic front textures for tandem thin-film silicon solar cells," *IEEE J. Photovolt.*, vol. 4, no. 5, pp. 1177–1184, Sep. 2014.

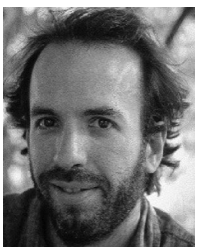

Federico Ventosinos received the Ph.D. degree in physics from the Universidad del Litoral, Santa Fe, Argentina, in 2013, working in different characterization techniques for amorphous semiconductors.

After the Ph.D., he did one year of postdoctoral studies at Laboratoire Génie électrique et électronique de Paris, followed by a two year postdoc Fellow with the Laboratoire de Physique et Couches Minces, Ecole Polytechnique, Palaiseau, France. He is focused on advanced characterization techniques for semiconductors and solar cell devices.

Jan Klusáček received the Bachelor's degree in power electrical and electronic engineering from Vysoké učení technické, Brno, Czech Republic, in 2018.

He was a participant of a two-year project called Open Science at Institute of Physics, Academy of Sciences of The Czech Republic v. v. i in 2014–2015 while studying High School.

Tomáš Finsterle received the Graduate degree in intelligent buildings from the Faculty of Electrical Engineering, Czech Technical University, Prague, in 2013, on the topic "Changes in the parameters of thin-film photovoltaic modules." He is currently working toward the Doctoral degree at the same institution, working on diagnostics of PV systems and thin-film module characterization.

He is currently with the Laboratory of PV Systems Diagnostics, Faculty of Electrical Engineering, Czech Technical University, Prague, Czech Republic.

Karel Künzel received the Graduate degree in power electronics from Faculty of Electrical Engineering, Czech Technical University, Prague, Czech Republic, in 1982 and the Postgraduate degree from the same institution, working on microprocessor control of electric drives, in 1986.

He is currently with the Faculty of Electrical Engineering as a Lecturer. He participates in grant projects focused on electromagnetic compatibility of power systems and technology of electric drives.

Franz-Josef Haug received the Diploma in physics from the Universities of Ulm and Waikato in 1986 and received the Ph.D. degree from ETH Zrich, Zürich, Switzerland, in 2001, working on Cu(In,Ga)Se2 solar cells.

As Postdoc, he worked on plasma processes for hard coatings of TiN at Empa and later on surface modifications for transparent electrodes based on ZnO at the Jlich Research Centre. In 2005, he became group leader within the PV-Lab, University of Neuchâtel. Since 2009, the lab was integrated into EPFL, where he joined the faculty in 2013 as a Senior Lecturer and Researcher.

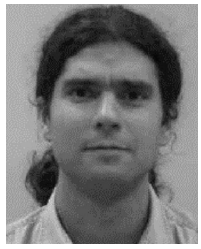

Jakub Holovský received the Ph.D. degree in quantum optics and optoelectronics from Charles University in Prague, Prague, Czech Republic, in 2012.

He pursued the scientific work at the Institute of Physics, Academy of Sciences, The Czech Republic v. v. i. and at Photovoltaics and Thin-Film Electronics Laboratory, Ecole Polytechnique Fédérale de Lausanne, Neuchâtel, Switzerland, where he also spent one year as a SCIEX Postdoc Fellow. Since 2018, he is Associate Professor at the Czech Technical University in Prague. He is focused on low absorption characterization methods for photovoltaic materials. Since 2017, he has been developing crystalline silicon solar cell technology adapted to low irradiances.